arXiv:1611.06893v3 [q-bio.NC] 23 Nov 2016

A statistical model for brain networks inferred from large-scale electrophysiological signals

Catalina Obando[a,b], Fabrizio De Vico Fallani[a,b,*]

[a]*Inria Paris, Aramis project-team, 75013, Paris, France*
[b]*Sorbonne Universites, UPMC Univ Paris 06, Inserm, CNRS, Institut du cerveau et la moelle (ICM), Hopital Pitie-Salpetriere, 75013, Paris, France*

Abstract

Network science has been extensively developed to characterize structural properties of complex systems, including brain networks inferred from neuroimaging data.

As a result of the inference process, networks estimated from experimentally obtained biological data, represent one instance of a larger number of realizations with similar intrinsic topology. A modeling approach is therefore needed to support statistical inference on the bottom-up local connectivity mechanisms influencing the formation of the estimated brain networks.

Here, we adopted a statistical model based on exponential random graphs (ERGM) to reproduce brain networks, or connectomes, estimated by spectral coherence between high-density electroencephalographic (EEG) signals. ERGMs are made up by different local graph metrics whereas the parameters weight the respective contribution in explaining the observed network. We validated this approach in a dataset of $N = 108$ healthy subjects during eyes-open (EO) and eyes-closed (EC) resting-state conditions.

Results showed that the tendency to form triangles and stars, reflecting clustering and node centrality, better explained the global properties of the EEG connectomes as compared to other combinations of graph metrics. In particular, the synthetic networks generated by this model configuration replicated the characteristic differences found in the real brain networks, with EO eliciting significantly higher segregation in the *alpha* frequency band ($8 - 13$ Hz) as compared to EC. Furthermore, the fitted ERGM parameter values provided complementary information showing that clustering connections are significantly more represented from EC to EO in the *alpha* range, but also in the *beta* band ($14 - 29$ Hz), which is known to play a crucial role in cortical processing of visual input and externally oriented attention.

Taken together, these findings support the current view of the brain functional segregation and integration in terms of modules and hubs, and provide a statistical approach to extract new information on the (re)organizational mechanisms in healthy and diseased brains.

Keywords: `Exponential random graph models, Brain connectivity, Graph theory, EEG, Resting-states`

*Corresponding author

ICM, Hopital Pitie-Salpetriere
75013 Paris, France
Tel +33(0)157274294
Email fabrizio.devicofallani@gmail.com

1. Introduction

The study of the human brain at rest provides precious information that is predictive of intrinsic functioning, cognition, as well as pathology [1]. In the last decade, graph theoretic approaches have described the topological structure of resting-state connectomes derived from different neuroimaging techniques, such as functional magnetic resonance imaging (fMRI) or magneto (MEG) and electroencephalography (EEG).

These estimated connectomes, or brain networks, tend to exhibit similar organizational properties including small-worldness, cost-efficiency, modularity and node centrality [2], as well as characteristic dependence from the anatomical backbone connectivity [3–5] and genetic factors [6]. Furthermore, they show potentially clinical relevance as demonstrated by the recent development of network-based diagnostics of consciousness [7, 8], Alzheimer's disease [9], stroke recovery [10], and schizofrenia [11]. In this sense, quantifying topological properties of default-mode connectomes by means of graph theory has enriched our understanding of the structure of functional brain connectivity maps [2, 12–14]. Nevertheless, these results refer to a descriptive analysis of the observed brain network, which is only one instance of several alternatives with similar structural features. This is especially true for functional networks inferred from empirically obtained data, where the edges (or links) are noisy estimates of the true connectivity and thresholding is often adopted to filter the relevant interactions between the system units [15–17].

Statistical models are therefore needed to reflect the uncertainty associated with a given observation, to permit inference about the relative occurrence of specific local structures, and to relate local-level processes to global-level properties [18]. A first approach consists in generating synthetic random networks that preserve some observed properties, such as the degree distribution or the random walk distribution, and then contrasting the values of the graph indices obtained in these synthetic networks with those extracted from the estimated connectomes [13]. While these methods often provide appropriate null models, and can improve the identification of relevant network properties [19–21], they do not inform on the organizational mechanisms modeling the whole network formation [22, 23]. Alternative approaches consider probabilistic growth models such as those based on spatial distances between nodes [24]. Interesting results have been achieved in identifying some basic connectivity rules reproducing both structural and functional brain networks [25, 26]. However, these methods suffer from the rough approximation (e.g., Euclidean) of the actual spatial distance between nodes, and moreover, they do not indicate if the identified local mechanisms are either necessary or sufficient as descriptors of the global network structure.

To support inference on the processes influencing the formation of network structure, statistical models have been conceived to consider the set of all possible alternative networks weighted on their similarity to the observed one [18]. Among others, exponential random graph model (ERGMs) represent a flexible category allowing to simultaneously assess the role of specific graph features on the formation of the entire network. These models have been first proposed as an extension of the triad model defined by [27] to characterize Markov graphs [28, 29] and have been widely developed to understand how simple interaction rules, such as transitivity, could give rise to the complex network of social contacts [30–38].

Recently, the use of ERGM has been proved to successfully model imaging connectomes derived respectively from spontaneous fMRI activity [39] and diffusion tensor

imaging (DTI) [40]. Despite its potential, the use of ERGM in network neuroscience is still in its infancy and more evidence is needed to better elucidate its applicability to connectomes inferred from other types of neuroimaging data and across different experimental conditions. In addition, many methodological issues remain unanswered, like for example the relationships between the graph metrics included in the ERGM and the graph indices used to describe the topology of the observed connectomes.

To address the above issues, we proposed and evaluated several ERGM configurations based on the combination of different local connectivity structures (i.e., graph metrics). Specifically, we modeled brain networks estimated from high-density EEG signals in a group of healthy individuals during eyes-open (EO) and eyes-closed (EC) resting-states. Our goal was to identify the best ERGM configuration reproducing EEG-derived connectomes in terms of functional integration and segregation, and to evaluate the ability of the estimated ERGM parameters in providing new information discriminating between EO and EC conditions.

2. Methods

2.1. EEG data and brain network construction

We used high-density EEG signals freely available from the online PhysioNet BCI database [41, 42]. EEG data consisted of one minute resting-state with eyes-open (EO) and one minute resting-state with eyes-closed (EC) recorded from 56 electrodes in 108 healthy subjects. EEG signals were recorded with an original sampling rate of 160Hz. All the EEG signals were referenced to the mean signal gathered from electrodes on the ear lobes. We subsequently downsampled the EEG signals to 100Hz after applying a proper anti-aliasing low-pass filter. The electrode positions on the scalp followed the standard 10-10 montage.

We used the spectral coherence [43] to measure functional connectivity (FC) between EEG signals of sensors i and j at a specific frequency band f as follows:

$$w_{ij}(f) = \frac{\mid S_{ij}(f) \mid^2}{S_{ii}(f)S_{jj}(f)} \tag{1}$$

Where S_{ij} is the cross-spectrum between i and j, and S_{ii} and S_{jj} the autospectra of i and j respectively. Specifically, we computed cross- and auto-spectra by means of the Welch's averaged modified periodogram with a sliding Hanning window of 1s and 0.5 seconds of overlap. The number of FFT points was set to 100 for a frequency resolution of 1Hz. As a result, we obtained for each subject a connectivity matrix $W(f)$ of size 56×56 where the entry $w_{ij}(f)$ contains the value of the spectral coherence between the EEG signals of sensors i and j at the frequency f.

We then averaged the connectivity matrices within the characteristic frequency bands *theta* $(4 - 7$ Hz), *alpha* $(8 - 13$ Hz), *beta* $(14 - 29$ Hz), *gamma* $(30 - 40$ Hz). These matrices constituted our raw brain networks whose nodes corresponded to the EEG sensors ($n = 56$) and links corresponded to the w_{ij} values. Finally, we thresholded the values in the connectivity matrices to retain the strongest links in each brain network. Specifically, we adopted an objective criterion, i.e., the efficiency cost optimization, to filter and binarize a number of links such that the final average node degree $k = 3$ [44]. We also considered $k = 1, 2, 4, 5$ to evaluate the main brain network properties around

the representative threshold $k = 3$. The resulting sparse brain networks, or graphs, were represented by adjacency matrices A, where each entry indicates the presence $a_{ij} = 1$ or absence $a_{ij} = 0$ of a link between nodes i and j.

2.2. Graph indices

We evaluated the global structure of brain networks by measuring graph indices at large-scale topological scales. We focused on well-known properties of brain networks such as optimal balance between integration and segregation of information [2, 45, 46]. Integration is the tendency of the network to favor distributed connectivity among remote brain areas; conversely, segregation is the tendency of the network to maintain connectivity within specialized groups of brain areas [47].

In graph theory integration has been typically quantified by the global-efficiency E_g and by the characteristic path length L:

$$\begin{aligned} E_g &= \frac{1}{n(n-1)} \sum_{i,j=1, i\neq j}^{n} \frac{1}{d_{ij}} \\ L &= \frac{1}{n(n-1)} \sum_{i,j=1, i\neq j}^{n} d_{ij} \end{aligned} \tag{2}$$

Where d_{ij} is the distance, or the length of the shortest path, between nodes i and j [48, 49].

Segregation is typically measured by means of the local-efficiency E_l and by the clustering coefficient C:

$$\begin{aligned} E_l &= \frac{1}{n} \sum_{i=1}^{n} E_g(G_i) \\ C &= \frac{1}{n} \sum_{i=1}^{n} \frac{2t_i}{k_i(k_i-1)} \end{aligned} \tag{3}$$

where G_i is the subgraph formed by the nodes connected to i; t_i is the number of triangles around node i, and k_i is the degree of node i [48, 49].

In addition, we evaluated the strength of division of a network into modules by measuring the modularity Q:

$$Q = \frac{1}{l} \sum_{i,j=1}^{n} \left(A_{ij} - \frac{k_i k_j}{l} \right) \delta_{m_i, m_j} \tag{4}$$

where $l = \sum_{i,j=1}^{n} A_{ij}$ is the number of edges, m_i is the module containing node i, and $\delta_{m_i,m_j} = 1$ if $m_i = m_j$ and 0 otherwise [50]. This metric can be seen as a compact measure of the integration and segregation of a network, as it measures the propensity to form dense connections between nodes within modules (i.e., segregation) but sparse connections between nodes in different modules (i.e., inverse of integration).

2.3. Exponential random graph model (ERGM)

Let G be a graph in a set $\mathcal{G}$ of possible network realizations, $g = [g_1, g_2, ..., g_r]$ be a vector of graph statistics, or metrics, and $g^* = [g_1^*, g_2^*, ..., g_r^*]$ the values of these metrics measured over G. Then, we can statistically model G by defining a probability distribution $P(G)$ over $\mathcal{G}$ such that the following conditions are satisfied:

$$\sum_{G \in \mathcal{G}} P(G) = 1 \tag{5}$$

$$\langle g_i \rangle = \sum_{G \in \mathcal{G}} g_i(G) P(G) = g_i^*, \quad i = \{1, 2, ..., r\} \tag{6}$$

where $\langle g_i \rangle$ is the expected value of the $i-th$ graph metric over $\mathcal{G}$.

By maximizing the Gibbs entropy of $P(G)$ constrained to the above conditions, the probability distribution reads as:

$$P(G) = \frac{e^{H(G)}}{Z} \tag{7}$$

where $H(G) = \sum_{i=1}^{r} \theta_i g_i(G)$ is the graph Hamiltonian, θ_i is the $i-th$ model parameter to be estimated and $Z = \sum_{G \in \mathcal{G}} e^{H(G)}$ is the so-called partition function [51]. The estimated value of a parameter θ_i indicates the change in the (log-odds) likelihood of an edge for a unit change in graph metric g_i. If the estimated value of θ_i is large and positive, the associated graph metric g_i plays an important role in explaining the topology of G more than would expected by chance. Notice that here chance corresponds to randomly choosing a network from the space $\mathcal{G}$. If instead the estimated value of θ_i is negative and large then g_i still plays an important role in explaining the topology of G but is less prevalent than expected by chance [52].

In general, the fact that the space $\mathcal{G}$ can be very large even for relatively small n, as well as the inclusion of graph metrics that are not simple linear combinations of G_{ij}, makes in practice impossible to derive analytically the model parameters vector $\boldsymbol{\theta} = [\theta_1, \theta_2, ..., \theta_r]$ [27, 31].

Numerical methods, such as Markov chain Monte Carlo (MCMC) approximations of the maximum likelihood estimators (MLE) of the model parameters vector $\boldsymbol{\theta}$ are typically adopted to circumvent this issue [53].

2.3.1. Model construction and implementation

We considered graph metrics reflecting basic properties of complex systems such as hub propensity and transitivity in the network [46, 54, 55]. Specifically, we focused on k-stars to model highly connected nodes (hubs) and k-triangles to model transitivity, where k refers to the order of the structures as illustrated in Fig. 1.

In general, this leads to a large number of model parameters to be estimated, i.e., $n-1$ for k-stars and $n-2$ for k-triangles. To avoid consequent degeneracy issues in the ERGM estimation, we adopted a compact specification for those metrics that combines them in an alternating geometric sequence [31, 56].

Because k-stars are related to the node degree distribution D [33], we used the *geometrically weighted degree distribution* GW_K as a graph metric to characterize hub propensity:

$$GW_K = e^{2\tau} \sum_{i=1}^{n-1} ((1 - e^{-\tau})^i - 1 + ie^{-\tau}) D_i \tag{8}$$

where $\tau > 0$ is a *ratio parameter* to penalize nodes with extremely high node degrees.

Similarly, because k-triangles are related to the *shared pattern distribution* S, we used the *geometrically weighted edgewise shared partner distribution* to characterize transitivity:

$$GW_E = e^{\tau} \sum_{i=1}^{n-2} (1 - (1 - e^{-\tau})^i) S_i \tag{9}$$

where the element S_i is the number of dyads that are directly connected and that have exactly i neighbors in common.

In addition, complementary metrics have been defined based on the *shared partner distribution*:

GW_N: *geometrically weighted non-edgewise shared partner distribution* given by Eq. 9, with S_i considering exclusively dyads that are not connected,

GW_D: *geometrically weighted dyadwise shared partner distribution* given by Eq. 9, with S_i considering any dyad, connected or not.

The above specifications yield particular ERGMs that belong to the so-called curved exponential family [33] and that have been extensively used in social science [32, 57, 58].

We constructed different ERGMs configurations by including these graph metrics as illustrated in Table 1. For the sake of simplicity, we only considered combinations of two graph metrics at most, except in one case where we also included the number of edges as a further metric [39, 40].

We tested the different configurations by fitting ERGM to brain networks in each single subject ($N = 108$), frequency band (*theta*, *alpha*, *beta*, *gamma*), and condition (EO, EC). To fit ERGMs we used a Markov chain Monte Carlo (MCMC) algorithm (Gibbs sampler) that samples networks from an exponential graph distribution. Specifically, we set the initial values of the model parameters $\boldsymbol{\theta^0}$ by means of a maximum pseudo-likelihood estimation (MPLE) [53, 59]. Then, we adopted the Fisher's scoring method to update the model parameters $\boldsymbol{\theta}$ until they converge to the approximated maximum likelihood estimators (MLEs) $\hat{\theta}$ [31]. As we used curved exponential random graph models, the ratio parameters τ were not fixed but were estimated as well.

Eventually, for each fitted ERGM configuration we generated 100 synthetic networks in order to obtain appropriate confidence intervals.

2.3.2. Goodness of fit

First, we used the Akaike information criterion (AIC) to evaluate relative quality of the ERGMs' fit by taking into account the maximum value of the likelihood function and the number of model parameters [60].

We also adopted a different approach to assess the absolute quality of the fit by comparing the synthetic networks generated by the estimated ERGMs and the observed brain networks. Specifically, we defined the following score based on the integration and segregation properties of networks:

$$\delta(E_g, E_l) = max\left(\mid \eta_{E_g} \mid, \mid \eta_{E_l} \mid\right) \tag{10}$$

Where η_{E_g}, η_{E_l} are the relative errors between the mean values of global/local efficiency of the simulated networks and the value of the observed brain network. By selecting the maximum absolute error we then considered the worse case similar to what have been proposed in [26]. Based on the above criteria, we selected the best model, which minimizes the AIC and δ mean values. To validate the model adequacy (Eq.6) we computed the Z-scores between the graph metrics' values of brain networks and synthetic networks.

Furthermore, we cross-validated the best model configuration by evaluating the synthetic networks' fitness to graph indices that were explicitly included neither in the ERGM nor in the model selection. We computed Pearson's correlation coefficient between the values of the characteristic path length (L), clustering coefficient (C) and modularity (Q) extracted from the observed brain networks and the mean values obtained from the corresponding simulated networks.

2.4. Statistical group analysis

We used non-parametric permutation t-tests to assess statistical differences between the values of the graph indices extracted from the brain networks in EO and EC resting state conditions. We also computed between-condition differences using the synthetic networks fitted by the best ERGMs. In this case, we considered the mean values of the graph indices in order to have one value corresponding to one brain network. For each test, we fixed a statistical threshold of $\alpha = 0.001$ and 100000 permutations.

3. Results

3.1. Characteristic functional segregation of EEG resting-state networks

The group-analysis revealed a significant increase of the local-efficiency in EO, as compared to EC, for the *alpha* band ($T = 3.529, p = 0.0007$, Fig. 2). We also reported a significant increment ($T = 3.557, p = 0.0007$) for the modularity in the *alpha* band, while no other statistically significant differences were observed in the other frequency bands, graph indices or metrics (Table S3). These differences were obtained for brain networks thresholded with an average node degree $k = 3$. Because similar differences were observed for some larger threshold values, we used $k = 3$ as a representative threshold in the rest of the study (Fig. S1).

We could not establish univocal relationships between E_g and E_l values and the metrics' values used in the ERGMs (Table S1). This was especially true for the global-efficiency, which exhibited significantly high correlations with all the other graph metrics (Spearman's $\mid R \mid > 0.43, p < 10^{-39}$).

3.2. Triangles and stars as fundamental constituents of functional brain networks

All the proposed ERGM configurations exhibited a relatively good fitting in terms of AIC, except for M_{11} (Fig. S2). Notably, the latter was the only configuration where the number of edges was considered as a model parameter and not as a constraint. M_1 gave the lowest $\delta(E_g, E_l)$ scores as compared to other configurations in both EO and EC conditions (Fig. 3). Notably, the configurations giving lower $\delta(E_g, E_l)$ scores included, directly or indirectly, the metric GW_E, with the exception of M_{11}.

We selected M_1 as a potentially good candidate to model EEG-derived brain networks. According to this model configuration the mass probability density reads $P(G) = Z^{-1}exp\{\theta_1 GW_E + \theta_2 GW_K\}$. The group-median values of the estimated parameters (θ_1 and θ_2) were all positive and larger than 1 in each band and condition (Table 2). This means that the likelihood of an edge to exist in a simulated network is larger if that edge is part of a triangle (GW_E) or of a star (GW_K) and that these connectivity structures are statistically relevant for the brain network formation.

Overall, the GW_E and GW_K values of the synthetic networks generated by M_1 were not significantly different from those of the observed brain networks (Fig. 4). This was true in every subject for GW_E ($Z < 2.58$, $p > 0.01$) and in at least the 94% of the subjects GW_K ($Z < 2.58$, $p > 0.01$). Furthermore, the values of the characteristic path length (L), clustering coefficient (C) and modularity (Q), extracted from synthetic networks were significantly correlated (Pearson's $R > 0.44, p < 10^{-6}$) with those of the brain networks in each frequency band (Fig. 5,Table S2). These results confirmed that M_1 adequately models EEG brain networks.

3.3. Simulating network differences between absence or presence of visual input

Fig. 6 illustrates the brain networks for a representative subject in the *alpha* band along with corresponding synthetic networks generated by M_1. In both EO and EC conditions, simulated networks and brain networks share similar topological structures characterized by diffused regularity and more concentrated connectivity in parietal and occipital regions.

The group-analysis over the synthetic networks revealed the ability of M_1 to capture not only individual properties of brain networks, but also the main observed difference between EC and EO resting-states, reflecting respectively absence and presence of visual input. Similarly to observed brain networks, we obtained, for simulated networks, a significant increase of the local-efficiency from EC to EO, in the *alpha* band ($T = 3.168, p = 0.002$). No other significant differences were reported in any other band or graph index/metric, including the modularity Q which only exhibited a marginal increase (Table S3).

Finally, by looking at the values of the estimated parameters, we observed that θ_1 values were significantly larger in EO compared to EC for both *alpha* ($T = 3.746, p = 0.0002$) and *beta* ($Z = 1.514, p = 0.0009$) frequency bands, while no significant differences were found for θ_2 values (Table 2).

4. Dicussion

In the last years, the use of statistical methods to infer the structure of complex systems has gained increasing interest [39, 61–63]. Beyond the descriptive characterization of networks, statistical network models (SNM) aim to statistically assess the local

connectivity processes involved in the global structure formation [18]. This is a crucial advance with respect to standard descriptive approaches because imaging connectomes, as other biological networks, are often inferred from experimentally obtained data and therefore the estimated edges can suffer from statistical noise and uncertainty [64].

In our study, we used ERGMs to identify the local connectivity structures that statistically form the intrinsic synchronization of large-scale electrophysiological activities. This model formulation has the advantage of statistically infer the probability of edge formation accounting for highly dependent configurations, such as transitivity structures, something lacking for example in the Bernoulli model. Furthermore, it is possible to include, in theory, graph metrics measuring global and local properties and discriminating node and edges attributes, such as homophily effects. In addition, it generalizes well-known networks models such as the stochastic block-model, where a block structure is imposed by including the count of edges between groups of nodes as a model metric [65].

Here, results showed that the tendency to form triangles (GW_E) and stars (GW_K) were sufficient to statistically reproduce the main properties of the EEG brain networks, such as functional integration and segregation, measured by means of global- E_g and local-efficiency E_l (Table S3). Our findings partially deviate from previous studies having adopted an ERGM to model fMRI and DTI brain networks, where GW_E and the geometrically weighted non-edgewise shared partner GW_N were selected under the assumption that these could be related respectively to local- and global-efficiency [39, 40]. However, here we showed that an univocal relationship between the ERGM graph indices and the metrics used to describe the EEG connectomes could not be statistically established (Table S1). While the propensity to form triangles (GW_E) can lead to cohesive clustering in the network (E_l), the propensity to form redundant paths of length 2 (i.e., GW_N) is not clearly related to the formation of short paths between nodes (E_g) [56]. Thus, while in general a good fit can be achieved including GW_N in the ERGM, the subsequent interpretation in terms of brain functional integration appears less straightforward. Here, we showed that GW_E together with the tendency to form stars (GW_K), rather gave the best fit in terms of local- and global-efficiency. Triangles and stars, giving rise to clustering and hubs, are fundamental building blocks of complex systems reflecting important mechanisms such as transitivity [48] and preferential attachment [66]. Notably, the existence of highly connected nodes is compatible with the presence of short paths (e.g., in a star graph the characteristic path length $L = 2$). This supports the recent view of the brain functional integration where segregated modules exchange information through central hubs and not necessarily through shortest paths [67, 68].

In the cross-validation phase, the selected model configuration captured other important brain network properties as measured by the clustering coefficient C, the characteristic path length L, and the modularity Q (Fig. 5). In terms of differences between conditions, the simulated networks gave a significant increase ($p < 0.001$) of E_l in the *alpha* band during EO as compared to EC, while, differently from observed brain networks, only marginal differences were reported for the modularity Q (Table S3). The latter could be in part ascribed to the absence of specific metrics in the ERGM accounting for modularity. In such respect, stochastic block models, which explicitly force modular structures, could represent an interesting alternative to explore in the future [69, 70]. Here, the increased *alpha* local-efficiency suggests a modulation of augmented specialized information processing, from EC to EO, that is consistent with typical global power reduction and increased regional activity [71]. Possible neural mechanisms explaining this

effect have been associated to automatic gathering of non-specific information resulting from more interactions within the visual system [72] and to shifts from interoceptive towards exteroceptive states [73–75].

As a crucial result, we provided complementary information by inspecting the fitted ERGM parameters. The positive $\theta_1 > 1$ and $\theta_2 > 1$ values indicated that both GW_E and GW_K are fundamental connectivity features that emerge in brain networks more than expected by chance (Table 2). However, only θ_1 values showed a significant difference (EO>EC) in the *alpha* band, as well as in the *beta* band (Table 2), suggesting that the tendency to form triangles, rather than the tendency to form stars, is a discriminant feature of eyes-closed and eyes-closed modes. More concentrated EEG activity among parieto-occipital areas has been largely documented in the *alpha*, but also in *beta* band, the latter reflecting either cortical processing of visual input or externally oriented attention [71, 76]. Notably, the role of the *beta* band could be found neither when analyzing brain networks nor synthetic networks (Fig.2, TableS3) and we speculate that this result specifically stems from the inherent ability of ERGMs to account for potential interaction between different graph metrics [56].

4.1. Methodological considerations

We estimated EEG connectomes by means of spectral coherence. While this measure is known to suffer from possible volume conduction effects [77], it has been also demonstrated that, probably due to this effect, it has the advantage of generating connectivity matrices highly consistent within and between subjects [78]. In addition, spectral coherence is still one of the most used measures to infer functional connectivity in the electrophysiological literature of resting-states because of its simplicity and relatively intuitive interpretation. Thus, constructing EEG connectomes by means of spectral coherence allowed us to better contextualize the results obtained with ERGM from a neurophysiological perspective. Future studies will have to assess if and how different connectivity estimators affect the choice of the model parameters.

Finally, we used a density-based thresholding procedure to filter information in the EEG raw networks by retaining and binarizing the strongest edges. Despite the consequent information loss, thresholding is often adopted to mitigate the uncertainty of the weakest edges, reduce the false positives, and facilitate the interpretation of the inferred network topology [13, 17]. The adopted criterion led to sparse brain networks and causes possible nodes to be disconnected. However, it has demonstrated empirically that the size of the resulting largest component typically contains more than the 60% of the brain nodes, thus ensuring a meaningful network structure [44].

Acknowledgments

We are grateful to M. Chavez and J. Guillon for their useful comments and suggestions. This work has been partially supported by the program "Investissements d'avenir" ANR-10-IAIHU-06.

References

[1] M. E. Raichle, A. M. MacLeod, A. Z. Snyder, W. J. Powers, D. A. Gusnard, G. L. Shulman, A default mode of brain function, PNAS 98 (2) (2001) 676–682. doi:10.1073/pnas.98.2.676.

[2] E. Bullmore, E. Bullmore, O. Sporns, O. Sporns, Complex brain networks: graph theoretical analysis of structural and functional systems, Nat Rev Neurosci 10 (maRcH) (2009) 186–198. doi:10.1038/nrn2575.
[3] C. J. Honey, O. Sporns, L. Cammoun, X. Gigandet, J. P. Thiran, R. Meuli, P. Hagmann, Predicting human resting-state functional connectivity from structural connectivity, PNAS 106 (6) (2009) 2035–2040. doi:10.1073/pnas.0811168106.
[4] G. Deco, A. Ponce-Alvarez, D. Mantini, G. L. Romani, P. Hagmann, M. Corbetta, Resting-state functional connectivity emerges from structurally and dynamically shaped slow linear fluctuations, J. Neurosci. 33 (27) (2013) 11239–11252. doi:10.1523/JNEUROSCI.1091-13.2013.
[5] H.-J. Park, K. Friston, Structural and Functional Brain Networks: From Connections to Cognition, Science 342 (6158) (2013) 1238411. doi:10.1126/science.1238411.
[6] A. Fornito, A. Zalesky, D. S. Bassett, D. Meunier, I. Ellison-Wright, M. Ycel, S. J. Wood, K. Shaw, J. O'Connor, D. Nertney, B. J. Mowry, C. Pantelis, E. T. Bullmore, Genetic influences on cost-efficient organization of human cortical functional networks, J. Neurosci. 31 (9) (2011) 3261–3270. doi:10.1523/JNEUROSCI.4858-10.2011.
[7] S. Achard, C. Delon-Martin, P. E. Vrtes, F. Renard, M. Schenck, F. Schneider, C. Heinrich, S. Kremer, E. T. Bullmore, Hubs of brain functional networks are radically reorganized in comatose patients, PNAS 109 (50) (2012) 20608–20613. doi:10.1073/pnas.1208933109.
[8] S. Chennu, P. Finoia, E. Kamau, J. Allanson, G. B. Williams, M. M. Monti, V. Noreika, A. Arnatkeviciute, A. Canales-Johnson, F. Olivares, D. Cabezas-Soto, D. K. Menon, J. D. Pickard, A. M. Owen, T. A. Bekinschtein, Spectral Signatures of Reorganised Brain Networks in Disorders of Consciousness, PLOS Computational Biology 10 (10) (2014) e1003887. doi:10.1371/journal.pcbi.1003887.
[9] B. M. Tijms, A. M. Wink, W. de Haan, W. M. van der Flier, C. J. Stam, P. Scheltens, F. Barkhof, Alzheimer's disease: connecting findings from graph theoretical studies of brain networks, Neurobiology of Aging 34 (8) (2013) 2023–2036. doi:10.1016/j.neurobiolaging.2013.02.020.
[10] C. Grefkes, G. R. Fink, Reorganization of cerebral networks after stroke: new insights from neuroimaging with connectivity approaches, Brain 134 (5) (2011) 1264–1276. doi:10.1093/brain/awr033.
[11] M.-E. Lynall, D. S. Bassett, R. Kerwin, P. J. McKenna, M. Kitzbichler, U. Muller, E. Bullmore, Functional Connectivity and Brain Networks in Schizophrenia, J. Neurosci. 30 (28) (2010) 9477–9487. doi:10.1523/JNEUROSCI.0333-10.2010.
[12] C. Stam, Functional connectivity patterns of human magnetoencephalographic recordings: a small-world network?, Neuroscience Letters 355 (1-2) (2004) 25–28. doi:10.1016/j.neulet.2003.10.063.
[13] M. Rubinov, O. Sporns, Complex network measures of brain connectivity: uses and interpretations., NeuroImage 52 (3) (2010) 1059–69. doi:10.1016/j.neuroimage.2009.10.003.
[14] C. J. Stam, E. C. W. van Straaten, The organization of physiological brain networks, Clinical Neurophysiology 123 (6) (2012) 1067–1087. doi:10.1016/j.clinph.2012.01.011.
[15] M. Tumminello, T. Aste, T. D. Matteo, R. N. Mantegna, A tool for filtering information in complex systems, PNAS 102 (30) (2005) 10421–10426. doi:10.1073/pnas.0500298102.
[16] M. Vidal, M. Cusick, A.-L. Barabsi, Interactome Networks and Human Disease, Cell 144 (6) (2011) 986–998. doi:10.1016/j.cell.2011.02.016.
[17] F. De Vico Fallani, J. Richiardi, M. Chavez, S. Achard, P. T. R. S. B, Graph analysis of functional brain networks : practical issues in translational neuroscience Graph analysis of functional brain networks : practical issues in translational neuroscience (September).
[18] A. Goldenberg, A. X. Zheng, S. E. Fienberg, E. M. Airoldi, A survey of statistical network models, arXiv:0912.5410 [physics, q-bio, stat]ArXiv: 0912.5410.
[19] R. Milo, S. Shen-Orr, S. Itzkovitz, N. Kashtan, D. Chklovskii, U. Alon, Network Motifs: Simple Building Blocks of Complex Networks, Science 298 (5594) (2002) 824–827. doi:10.1126/science.298.5594.824.
[20] D. Garlaschelli, M. I. Loffredo, Patterns of link reciprocity in directed networks, Physical Review Letters 93 (26), arXiv: cond-mat/0404521. doi:10.1103/PhysRevLett.93.268701.
[21] M. D. Humphries, K. Gurney, Network Small-World-Ness: A Quantitative Method for Determining Canonical Network Equivalence, PLOS ONE 3 (4) (2008) e0002051. doi:10.1371/journal.pone.0002051.
[22] A.-L. Barabasi, H. Jeong, Z. Nda, E. Ravasz, A. Schubert, T. Vicsek, Evolution of the social network of scientific collaborations, Physica A: Statistical mechanics and its applications 311 (3) (2002) 590–614.
[23] M. E. J. Newman, D. J. Watts, S. H. Strogatz, Random graph models of social networks, PNAS 99 (suppl 1) (2002) 2566–2572. doi:10.1073/pnas.012582999.

[24] M. Barthlemy, Spatial networks, Physics Reports 499 (13) (2011) 1–101. doi:10.1016/j.physrep.2010.11.002.

[25] P. E. Vertes, A. F. Alexander-Bloch, N. Gogtay, J. N. Giedd, J. L. Rapoport, E. T. Bullmore, Simple models of human brain functional networks, PNAS 109 (15) (2012) 5868–5873. doi:10.1073/pnas.1111738109.

[26] R. F. Betzel, A. Avena-Koenigsberger, J. Goi, Y. He, M. A. de Reus, A. Griffa, P. E. Vrtes, B. Miic, J.-P. Thiran, P. Hagmann, M. van den Heuvel, X.-N. Zuo, E. T. Bullmore, O. Sporns, Generative models of the human connectome, NeuroImage 124, Part A (2016) 1054–1064. doi:10.1016/j.neuroimage.2015.09.041.

[27] O. Frank, D. Strauss, Markov graphs, Journal of the american Statistical 81 (395) (1986) 832–842. doi:10.2307/2289017.

[28] O. Frank, Statistical analysis of change in networks, Statistica Neerlandica 45 (3) (1991) 283–293. doi:10.1111/j.1467-9574.1991.tb01310.x.

[29] S. Wasserman, P. Pattison, Logit models and logistic regressions for social networks: I. An introduction to Markov graphs andp, Psychometrika 61 (3) (1996) 401–425. doi:10.1007/BF02294547.

[30] M. S. Handcock, Statistical models for social networks: Inference and degeneracy, na, 2002.

[31] D. R. Hunter, M. S. Handcock, Inference in Curved Exponential Family Models for Networks, Journal of Computational and Graphical Statistics 15 (3) (2006) 565–583. doi:10.1198/106186006X133069.

[32] S. M. Goodreau, Advances in exponential random graph (p*) models applied to a large social network, Social Networks 29 (39) (2007) 231–248. doi:10.1016/j.socnet.2006.08.001.

[33] D. R. Hunter, Curved exponential family models for social networks, Social Networks 29 (2007) 216–230. doi:10.1016/j.socnet.2006.08.005.

[34] A. Rinaldo, S. E. Fienberg, Y. Zhou, On the geometry of discrete exponential families with application to exponential random graph models, Electron. J. Statist. 3 (2009) 446–484. doi:10.1214/08-EJS350.

[35] G. Robins, P. Pattison, P. Wang, Closure, connectivity and degree distributions: Exponential random graph (p*) models for directed social networks, Social Networks 31 (2009) 105–117. doi:10.1016/j.socnet.2008.10.006.

[36] S. M. Goodreau, J. a. Kitts, M. Morris, Birds of a feather, or friend of a friend? Using exponential random graph models to investigate adolescent social networks., Demography 46 (1) (2009) 103–125. doi:10.1353/dem.0.0045.

[37] P. Wang, P. Pattison, G. Robins, Exponential random graph model specifications for bipartite networks-A dependence hierarchy, Social Networks 35 (2) (2013) 211–222. doi:10.1016/j.socnet.2011.12.004.

[38] A. M. Niekamp, L. a. G. Mercken, C. J. P. a. Hoebe, N. H. T. M. Dukers-Muijrers, A sexual affiliation network of swingers, heterosexuals practicing risk behaviours that potentiate the spread of sexually transmitted infections: A two-mode approach, Social Networks 35 (2) (2013) 223–236. doi:10.1016/j.socnet.2013.02.006.

[39] S. L. Simpson, S. Hayasaka, P. J. Laurienti, Exponential random graph modeling for complex brain networks., PloS one 6 (5) (2011) e20039–e20039. doi:10.1371/journal.pone.0020039.

[40] M. R. T. Sinke, R. M. Dijkhuizen, A. Caimo, C. J. Stam, W. M. Otte, Bayesian exponential random graph modeling of whole-brain structural networks across lifespan, NeuroImage 135 (2016) 79–91. doi:10.1016/j.neuroimage.2016.04.066.

[41] A. L. Goldberger, L. A. N. Amaral, L. Glass, J. M. Hausdorff, P. C. Ivanov, R. G. Mark, J. E. Mietus, G. B. Moody, C.-K. Peng, H. E. Stanley, PhysioBank, PhysioToolkit, and PhysioNet, Circulation 101 (23) (2000) e215–e220. doi:10.1161/01.CIR.101.23.e215.

[42] G. Schalk, D. J. McFarland, T. Hinterberger, N. Birbaumer, J. R. Wolpaw, BCI2000: a general-purpose brain-computer interface (BCI) system, IEEE Transactions on Biomedical Engineering 51 (6) (2004) 1034–1043. doi:10.1109/TBME.2004.827072.

[43] G. C. Carter, Coherence and time delay estimation, Proceedings of the IEEE 75 (2) (1987) 236–255. doi:10.1109/PROC.1987.13723.

[44] F. De Vico Fallani, V. Latora, M. Chavez, Filtering information in imaging connectomics, arXiv:1603.08445 [q-bio]ArXiv: 1603.08445.

[45] G. Tononi, O. Sporns, G. M. Edelman, A measure for brain complexity: relating functional segregation and integration in the nervous system., Proceedings of the National Academy of Sciences of the United States of America 91 (May) (1994) 5033–5037. doi:10.1073/pnas.91.11.5033.

[46] D. S. Bassett, E. Bullmore, Small-World Brain Networks, Neuroscientist 12 (6) (2006) 512–523. doi:10.1177/1073858406293182.

[47] K. J. Friston, Functional and effective connectivity: a review., Brain connectivity 1 (1) (2011) 13–36. doi:10.1089/brain.2011.0008.
[48] D. J. Watts, S. H. Strogatz, Collective dynamics of small-world networks, Nature 393 (6684) (1998) 440–442. doi:10.1038/30918.
[49] V. Latora, M. Marchiori, Efficient behavior of small-world networks., Physical review letters 87 (2001) 198701–198701. doi:10.1103/PhysRevLett.87.198701.
[50] M. E. J. Newman, Modularity and community structure in networks, PNAS 103 (23) (2006) 8577–8582. doi:10.1073/pnas.0601602103.
[51] M. Newman, Networks: An Introduction, Oxford University Press, 2010.
[52] G. Robins, P. Pattison, Y. Kalish, D. Lusher, An introduction to exponential random graph (p *) models for social networks, Social Networks 29 (2007) 173–191. doi:10.1016/j.socnet.2006.08.002.
[53] T. A. B. Snijders, Markov Chain Monte Carlo Estimation of Exponential Random Graph Models.
[54] L. a. N. Amaral, A. Scala, M. Barthlmy, H. E. Stanley, Classes of small-world networks, PNAS 97 (21) (2000) 11149–11152. doi:10.1073/pnas.200327197.
[55] X. F. Wang, G. Chen, Complex networks: small-world, scale-free and beyond, IEEE Circuits and Systems Magazine 3 (1) (2003) 6–20. doi:10.1109/MCAS.2003.1228503.
[56] P. P. Snijders, Robins GL & Handcock MS, New specifications for exponential random graph models (2006) 99–153doi:10.1111/j.1467-9531.2006.00176.x.
[57] G. Robins, T. Snijders, P. Wang, M. Handcock, P. Pattison, Recent developments in exponential random graph (p*) models for social networks, Social Networks 29 (2007) 192–215. doi:10.1016/j.socnet.2006.08.003.
[58] D. Lusher, J. Koskinen, G. Robins, Exponential Random Graph Models for Social Networks: Theory, Methods, and Applications, Cambridge University Press, 2012, google-Books-ID: gyKypohCjDcC.
[59] M. A. J. van Duijn, K. J. Gile, M. S. Handcock, A framework for the comparison of maximum pseudo-likelihood and maximum likelihood estimation of exponential family random graph models, Social Networks 31 (1) (2009) 52–62. doi:10.1016/j.socnet.2008.10.003.
[60] H. Akaike, Information Theory and an Extension of the Maximum Likelihood Principle, in: E. Parzen, K. Tanabe, G. Kitagawa (Eds.), Selected Papers of Hirotugu Akaike, Springer Series in Statistics, Springer New York, 1998, pp. 199–213, dOI: 10.1007/978-1-4612-1694-0_15.
[61] R. Guimer, M. Sales-Pardo, A Network Inference Method for Large-Scale Unsupervised Identification of Novel Drug-Drug Interactions, PLOS Computational Biology 9 (12) (2013) e1003374. doi:10.1371/journal.pcbi.1003374.
[62] T. Martin, B. Ball, M. E. J. Newman, Structural inference for uncertain networks, Physical Review E 93 (1), arXiv: 1506.05490. doi:10.1103/PhysRevE.93.012306.
[63] D. Hric, T. P. Peixoto, S. Fortunato, Network structure, metadata and the prediction of missing nodes and annotations, Physical Review X 6 (3), arXiv: 1604.00255. doi:10.1103/PhysRevX.6.031038.
[64] R. C. Craddock, S. Jbabdi, C.-G. Yan, J. T. Vogelstein, F. X. Castellanos, A. Di Martino, C. Kelly, K. Heberlein, S. Colcombe, M. P. Milham, Imaging human connectomes at the macroscale, Nat Meth 10 (6) (2013) 524–539. doi:10.1038/nmeth.2482.
[65] P. W. Holland, K. B. Laskey, S. Leinhardt, Stochastic blockmodels: First steps, Social networks 5 (2) (1983) 109–137.
[66] A.-L. Barabasi, R. Albert, Emergence of Scaling in Random Networks, Science 286 (5439) (1999) 509–512. doi:10.1126/science.286.5439.509.
[67] O. Sporns, Network attributes for segregation and integration in the human brain, Current Opinion in Neurobiology 23 (2) (2013) 162–171. doi:10.1016/j.conb.2012.11.015.
[68] G. Deco, G. Tononi, M. Boly, M. L. Kringelbach, Rethinking segregation and integration: contributions of whole-brain modelling, Nat Rev Neurosci 16 (7) (2015) 430–439. doi:10.1038/nrn3963.
[69] B. Karrer, M. E. J. Newman, Stochastic blockmodels and community structure in networks, Physical Review E 83 (1), arXiv: 1008.3926. doi:10.1103/PhysRevE.83.016107.
[70] D. M. Pavlovic, P. E. Vrtes, E. T. Bullmore, W. R. Schafer, T. E. Nichols, Stochastic Blockmodeling of the Modules and Core of the Caenorhabditis elegans Connectome, PLOS ONE 9 (7) (2014) e97584. doi:10.1371/journal.pone.0097584.
[71] R. J. Barry, A. R. Clarke, S. J. Johnstone, C. A. Magee, J. A. Rushby, EEG differences between eyes-closed and eyes-open resting conditions, Clinical Neurophysiology 118 (12) (2007) 2765–2773. doi:10.1016/j.clinph.2007.07.028.
[72] C. Yan, D. Liu, Y. He, Q. Zou, C. Zhu, X. Zuo, X. Long, Y. Zang, Spontaneous Brain Activity in the

Default Mode Network Is Sensitive to Different Resting-State Conditions with Limited Cognitive Load, PLOS ONE 4 (5) (2009) e5743. doi:10.1371/journal.pone.0005743.

[73] E. Marx, A. Deutschlnder, T. Stephan, M. Dieterich, M. Wiesmann, T. Brandt, Eyes open and eyes closed as rest conditions: impact on brain activation patterns, NeuroImage 21 (4) (2004) 1818–1824. doi:10.1016/j.neuroimage.2003.12.026.

[74] M. Bianciardi, M. Fukunaga, P. van Gelderen, S. G. Horovitz, J. A. de Zwart, J. H. Duyn, Modulation of spontaneous fMRI activity in human visual cortex by behavioral state, Neuroimage 45 (1) (2009) 160–168. doi:10.1016/j.neuroimage.2008.10.034.

[75] P. Xu, R. Huang, J. Wang, N. T. Van Dam, T. Xie, Z. Dong, C. Chen, R. Gu, Y.-F. Zang, Y. He, J. Fan, Y.-j. Luo, Different topological organization of human brain functional networks with eyes open versus eyes closed, NeuroImage 90 (2014) 246–255. doi:10.1016/j.neuroimage.2013.12.060.

[76] Y. A. Boytsova, S. G. Danko, EEG differences between resting states with eyes open and closed in darkness, Hum Physiol 36 (3) (2010) 367–369. doi:10.1134/S0362119710030199.

[77] R. Srinivasan, W. R. Winter, J. Ding, P. L. Nunez, EEG and MEG coherence: Measures of functional connectivity at distinct spatial scales of neocortical dynamics, Journal of Neuroscience Methods 166 (1) (2007) 41–52. doi:10.1016/j.jneumeth.2007.06.026.

[78] G. L. Colclough, M. W. Woolrich, P. K. Tewarie, M. J. Brookes, A. J. Quinn, S. M. Smith, How reliable are MEG resting-state connectivity metrics?, NeuroImage 138 (2016) 284–293. doi:10.1016/j.neuroimage.2016.05.070.

[79] J. T. Vogelstein, J. M. Conroy, V. Lyzinski, L. J. Podrazik, S. G. Kratzer, E. T. Harley, D. E. Fishkind, R. J. Vogelstein, C. E. Priebe, Fast Approximate Quadratic Programming for Large (Brain) Graph Matching, arXiv:1112.5507 [cs, math, q-bio]ArXiv: 1112.5507.

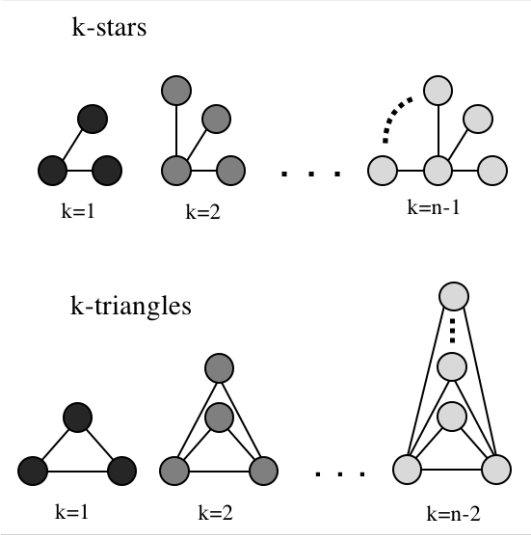

Figure 1: Graphical representation of $k-$stars and $k-$triangles

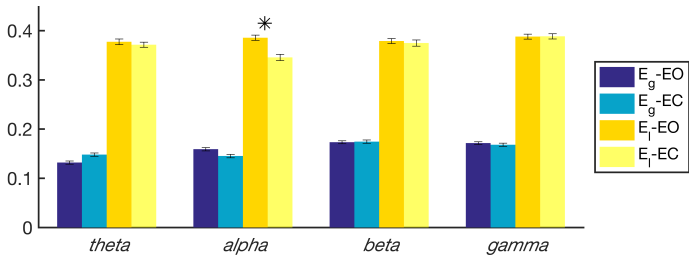

Figure 2: Median values and standard errors of global- and local-efficiency measured from EEG brain networks across 108 subjects in eyes-open (EO) and eyes-closed (EC) resting-states.
$*$ p-value < 0.001.

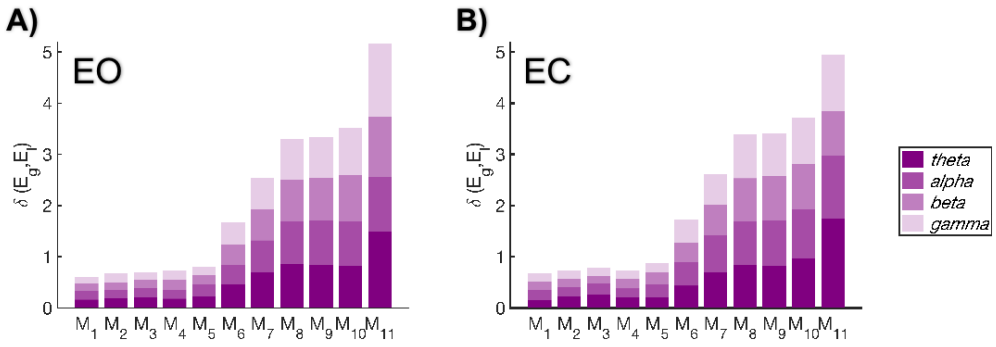

Figure 3: Absolute quality of ERG models' fit. Colored bars show the group-averaged cumulative errors $\delta(E_g, E_l)$ in terms of relative of global- and local-efficiency across frequency bands. Model configurations are listed on the x-axis. Panel A) illustrates values for eyes-open resting-state (EO); panel B) shows the error values for eyes-closed resting-state (EC).

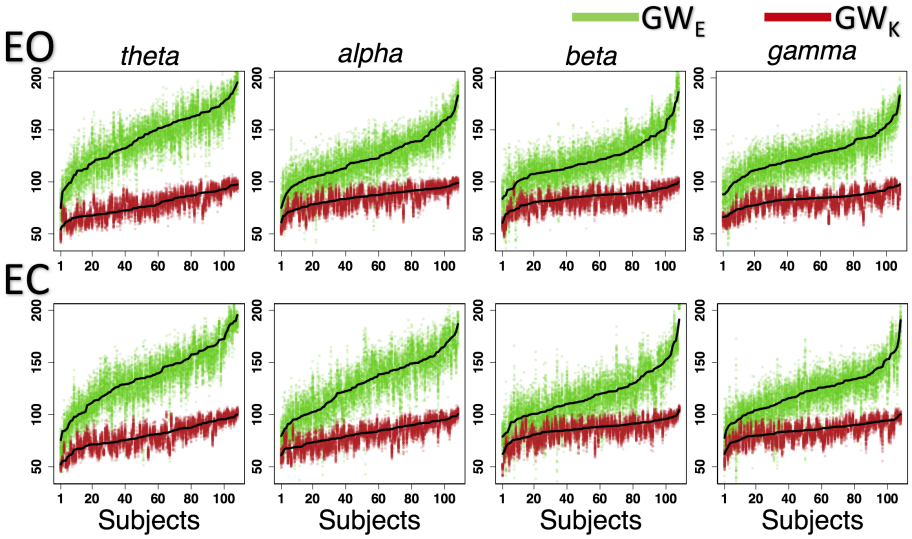

Figure 4: Adequacy of model configuration M_1. Green and red dots represent respectively the values of the *geometrically weighted edgewise shared pattern distribution* (GW_E) and *geometrically weighted degree distribution* (GW_K) measured in simulated networks. Black dots lines indicate the values measured in the observed brain networks.

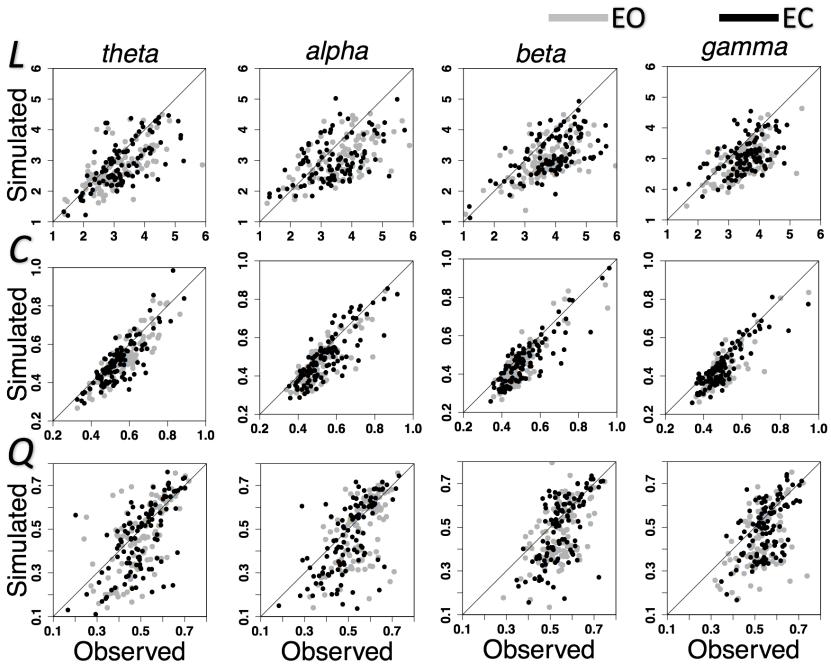

Figure 5: Cross-validation for model configuration M_1. Scatter plots show the values of the graph indices measured in the observed brain networks (x-axis) against the mean values obtained from synthetic networks (y-axis). Three graph indices were considered: characteristic path length (L), clustering coefficient (C) and modularity (Q). Grey dots correspond to eyes-open resting-states (EO); black dots correspond to eyes-closed resting-states (EC).

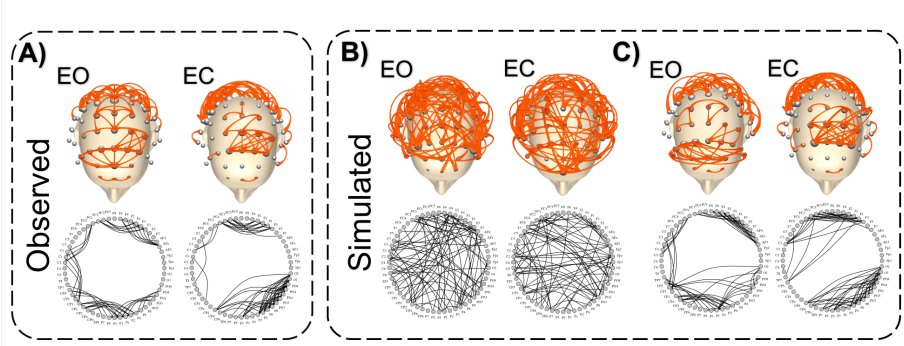

Figure 6: Brain networks and synthetic networks for a representative subject. Panel A): brain network in the *alpha* band for the eyes-open (EO) and eyes-closed (EC) resting-state. Panel B): one instance of the corresponding synthetic networks generated by model configuration M_1. Panel C): because node labels are not preserved in the simulated networks, we re-assigned them virtually by using the Frank-Wolfe algorithm [79], which optimizes the graph matching with the observed brain network. In the upper part of the figure, nodes correspond to EEG electrodes, whose position follows a standard $10-10$ montage. In the bottom part, the nodes are arranged into a circle.

Models	Edges	GW_K	GW_E	GW_N	GW_D
M_1	$*$	✓	✓	-	-
M_2	$*$	-	✓	-	✓
M_3	$*$	-	-	✓	✓
M_4	$*$	-	✓	✓	-
M_5	$*$	-	✓	-	-
M_6	$*$	-	-	✓	-
M_7	$*$	✓	-	✓	-
M_8	$*$	✓	-	-	✓
M_9	$*$	✓	-	-	-
M_{10}	$*$	-	-	-	✓
M_{11}	✓	-	✓	✓	-

Table 1: Set of model configurations. Models M_1 to M_{10} include at most two of the four considered graph metrics i.e., GW_K, GW_E, GW_N, GW_D. The metric "Edges" is fixed and equal to the actual number of edges in the observed brain networks in all the configurations but M_{11} model
$*$ Metrics that are fixed.
✓Metrics that are variable.

	θ_1			θ_2		
	EO	EC	$T(p)$	EO	EC	$T(p)$
theta	1.528(0.045)	1.531(0.039)	-0.281(0.7804)	1.502(0.169)	1.443(0.159)	-0.406 (0.690)
alpha	1.449(0.041)	1.297(0.039)	3.746(0.0002)	1.327(0.123)	1.317(0.532)	-1.084 (0.347)
beta	1.487(0.457)	1.326(0.046)	1.514(0.0009)	1.062(0.149)	1.303(0.169)	-0.890 (0.371)
gamma	1.552(0.046)	1.509(8.266)	-0.992(0.8521)	0.878(0.125)	1.140(3.002)	-1.064 (0.135)

Table 2: Statistics for the estimated parameters of the model configuration M_1. Median values and standard errors (within parentheses) are reported for the two resting-state conditions *EO* and *EC*. *T*-values and *p*-values (within parentheses) from non-parametric permutation-based t-tests between *EO* and *EC*, are shown in the third column of each subsection.

Supplementary Material

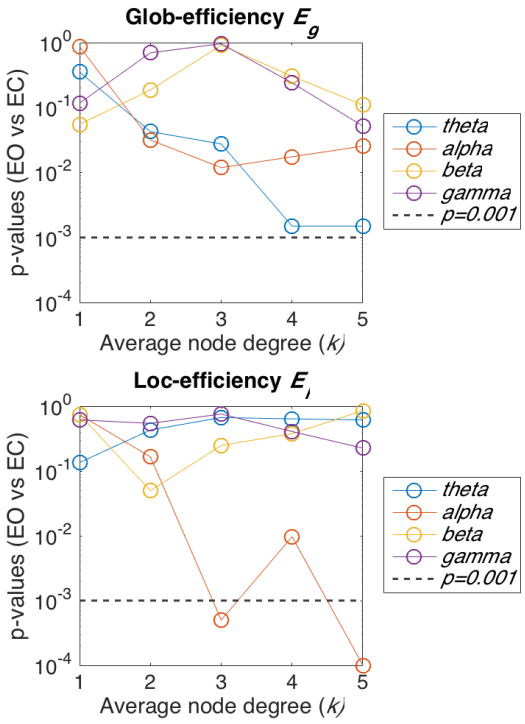

Figure S1: Statistical differences for global- and local-efficiency across different threshold values. p-values result from permutation t-tests between EO and EC conditions. Thresholds are shown as a function of the average node degree k. Five representative values have been selected for the sake of simplicity. $k = 3$ corresponds to the ECO criterion [44]

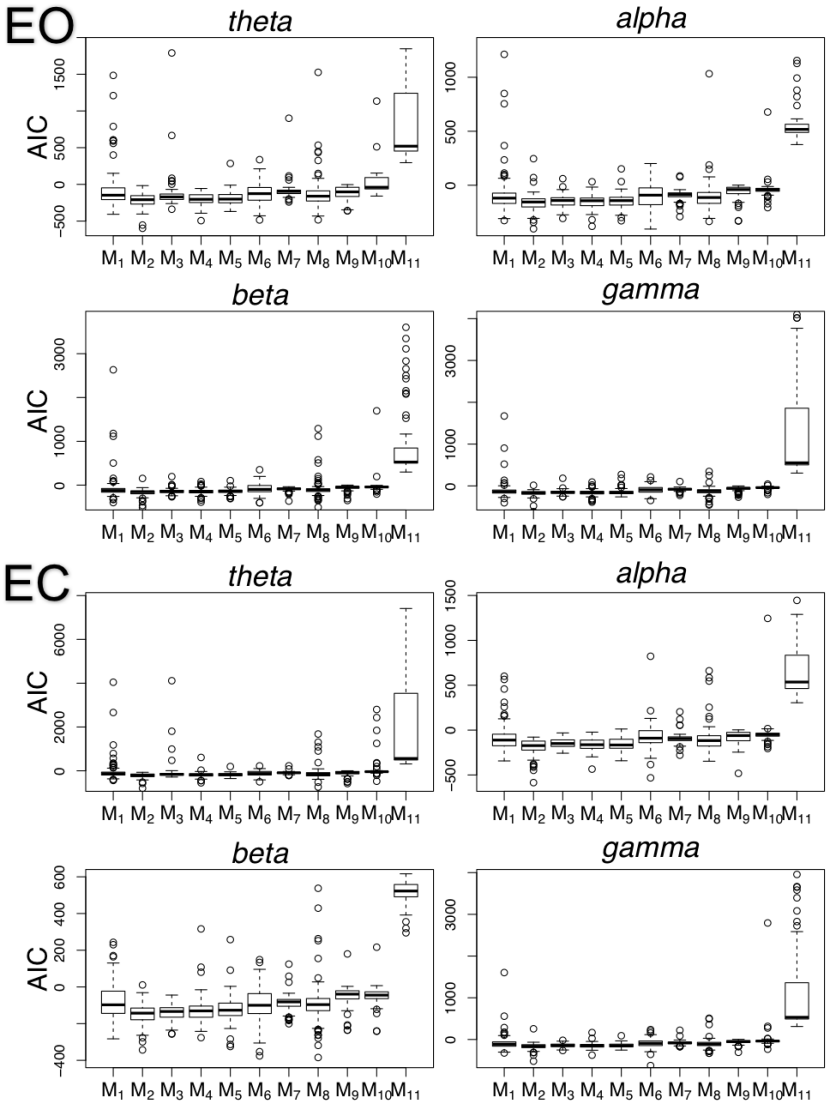

Figure S2: Box plots of the Akaike (AIC) values computed in each model configuration. Horizontal bold lines show the group medians. Circles denote outliers, bars indicate lower and upper quartiles, bars show the 5% and 95% percentiles.

	E_g		E_l	
	R	p-value	R	p-value
GW_K	0.601	$< 10^{-86}$	0.162	$< 10^{-6}$
GW_E	-0.832	$< 10^{-222}$	0.125	$< 10^{-4}$
GW_N	0.426	$< 10^{-39}$	-0.338	$< 10^{-24}$
GW_D	0.499	$< 10^{-55}$	-0.137	$< 10^{-5}$

Table S1: Statistical correlation between global- and local-efficiency, and graph metrics. Spearman's correlation coefficients, computed from the values of the pooled frequency bands, are reported along with the corresponding p-values.

	EO						**EC**					
	L		C		Q		L		C		Q	
	R	p-value	R	p-value	R	p-value	R	p-value	R	p-value	R	p-value
theta	0.642	$< 10^{-14}$	0.861	$< 10^{-33}$	0.684	$< 10^{-16}$	0.669	$< 10^{-15}$	0.834	$< 10^{-29}$	0.663	$< 10^{-15}$
alpha	0.589	$< 10^{-11}$	0.797	$< 10^{-25}$	0.552	$< 10^{-10}$	0.495	$< 10^{-8}$	0.840	$< 10^{-30}$	0.650	$< 10^{-14}$
beta	0.583	$< 10^{-11}$	0.875	$< 10^{-35}$	0.540	$< 10^{-9}$	0.638	$< 10^{-13}$	0.871	$< 10^{-34}$	0.618	$< 10^{-13}$
gamma	0.587	$< 10^{-11}$	0.794	$< 10^{-24}$	0.446	$< 10^{-6}$	0.490	$< 10^{-8}$	0.871	$< 10^{-34}$	0.559	$< 10^{-10}$

Table S2: Pearson's correlation coefficient between the values of the graph indices in the observed brain networks and the corresponding mean values obtained in simulated networks.

Observed										
	E_g $T(p)$	E_l $T(p)$	L $T(p)$	C $T(p)$	Q $T(p)$	GW_E $T(p)$	GW_N $T(p)$	GW_D T-(p)	GW_K $T(p)$
theta	-2.244(0.026)	0.404(0.688)	-1.059(0.291)	2.078(0.040)	-0.138(0.895)	1.751(0.085)	-1.415(0.158)	-1.771(0.081)	-1.307(0.195)
alpha	2.558(0.012)	3.529(0.0007)	2.113(0.035)	-2.298(0.024)	3.557(0.0007)	-2.073(0.043)	0.721(0.474)	2.186(0.033)	2.426(0.017)
beta	-0.091(0.931)	1.159(0.251)	-1.952(0.055)	-0.963(0.337)	-0.137(0.888)	0.986(0.330)	1.586(0.118)	2.198(0.030)	-1.370(0.172)
gamma	0.044(0.961)	-0.312(0.758)	-0.936(0.356)	-0.453(0.650)	-1.869(0.066)	1.437(0.151)	2.174(0.031)	1.967(0.052)	-2.077(0.040)
Simulated									
	E_g $T(p)$	E_l $T(p)$	L $T(p)$	C $T(p)$	Q $T(p)$	GW_E $T(p)$	GW_N $T(p)$	GW_D $T(p)$	GW_K $T(p)$
theta	-1.920(0.057)	0.178(0.862)	-1.255(0.211)	1.737(0.084)	-0.115(0.913)	1.730(0.086)	-0.968(0.338)	-0.908(0.371)	-0.986(0.327)
alpha	1.799(0.076)	3.168(0.002)	1.531(0.130)	-2.427(0.018)	1.661(0.097)	-2.086(0.040)	0.933(0.352)	1.032(0.310)	2.235(0.027)
beta	-0.861(0.393)	1.598(0.111)	-2.574(0.011)	-0.721(0.467)	-0.751(0.456)	1.491(0.139)	1.426(0.156)	1.885(0.061)	-1.529(0.130)
gamma	-0.645(0.520)	-0.683(0.494)	-2.134(0.034)	-1.063(0.290)	-2.236(0.028)	1.507(0.135)	2.147(0.035)	2.152(0.033)	-2.302(0.023)

Table S3: Statistical differences between the values of graph indices and metrics in the *EO* and *EC* condition. Upper part of the table shows the T-values and p-values (within parentheses) returned by non-parametric permutation-based t-tests between conditions in the observed brain networks. Bottom part of the table, shows the T-values and p-values (within parentheses) returned by non-parametric permutation-based t-tests between conditions in the simulated synthetic networks.